Tunnelling and Underground Space Technology 153 (2024) 106017

Contents lists available at ScienceDirect

Tunnelling and Underground Space Technology incorporating Trenchless Technology Research

journal homepage: www.elsevier.com/locate/tust

Enhancement of disposal efficiency for deep geological repositories based on three design factors – Decay heat optimization, increased thermal limit of the buffer and double-layer concept

Kwang-Il Kim [a,*], Changsoo Lee [a], Dongkeun Cho [b], Jonny Rutqvist [c]

[a] Disposal Safety Evaluation Research Division, Korea Atomic Energy Research Institute, 111 Daedeok Dae-Ro 989 Beon-Gil, Yuseong-gu, Daejeon 34057, Republic of Korea

[b] Research Center for Spent Nuclear Fuel Storage and Disposal, Korea Atomic Energy Research Institute, 111 Daedeok Dae-Ro 989 Beon-Gil, Yuseong-gu, Daejeon 34057, Republic of Korea

[c] Earth Sciences Division, Lawrence Berkeley National Laboratory, 1 Cyclotron Road, Berkeley, CA 94720, USA

ARTICLE INFO

Keywords:
Deep geological repository
Design factors
Disposal efficiency
Rock mass stability
Coupled thermo-hydro-mechanical modeling

ABSTRACT

This study investigates the enhancement of disposal efficiency for deep geological repositories (DGRs) based on three design factors: decay heat optimization, increased thermal limit of the buffer, and double-layer concept using coupled thermo-hydro-mechanical (THM) numerical simulations. Decay heat optimization is achieved by iteratively emplacing spent nuclear fuels having the maximum and minimum decay heat in a canister. Disposal areas can be reduced by 20 % to 40 % compared to the current reference disposal system in Korea (KRS^{+}) in accordance with the combinations of the three design factors, alleviating challenges in site selection for the DGR. This study additionally identifies an optimal layer spacing of 500 m for the double-layer concept in the viewpoint of the buffer temperature, where thermal interaction between the upper and lower layers nearly disappears. However, determining the ultimate disposal and layer spacing requires engineering judgement, considering not only the thermal performance of the DGR but also various factors such as cost and difficulties of the construction and rock mass stability. DGRs designed with an increased thermal limit of the buffer poses a greater probability of rock mass failure around disposal tunnels and deposition holes due to elevated thermal stresses. Densely arranged heat sources for the DGRs with enhanced disposal efficiency lead to larger temperature increase even at the far-field scale, raising a possibility of thermally driven fracture shear activation with associated hydraulic, mechanical, and seismic changes.

1. Introduction

Deep geological repository (DGR) is currently considered the most viable concept for isolating high-level radioactive waste (HLW) from living sphere of human beings (IAEA, 2003). The DGR concept employs a multi-barrier system that combines an engineered barrier system (EBS) and natural barrier system (NBS). The EBS materials, including a canister encapsulating spent nuclear fuels (SNFs), bentonite buffer, and backfill are placed in deposition holes and disposal tunnels. These materials provide mechanical stability to the SNFs, reducing physical impacts and prevent direct exposure of the SNFs to groundwater flowing from the near-field rock mass (Wersin et al., 2007; Rutqvist, 2020). The NBS indicating rock mass surrounding the DGR, will retard the transport of radionuclides if released and migrated out of the EBS materials (Kwon and Min, 2021; Zhang et al., 2022).

Bentonite is commonly chosen as a primary material for buffer and backfill due to its low permeability, high retention capacity for radionuclides, and swelling capability, which can seal gaps between the EBS materials and the surrounding rock mass (Zheng et al., 2015). Such characteristics of bentonite may be compromised by chemical alterations if the bentonite is exposed to high temperature resulting from decay heat and groundwater migrated from the near-field rock mass (Pusch and Karnland, 1996; Pusch et al., 2010; Wersin et al., 2007; Zheng et al., 2017). Most of the DGRs worldwide impose a thermal limit of 100 °C on the buffer to maintain its safety performance (Zheng et al., 2015; Ahonen et al., 2008; SKB, 2010; Lee et al., 2007).

Thermal limit of the buffer is one of the most important factors in DGR design, as it determines the spacings between disposal tunnels and

* Corresponding author.
E-mail address: kikim@kaeri.re.kr (K.-I. Kim).

https://doi.org/10.1016/j.tust.2024.106017
Received 26 February 2024; Received in revised form 9 July 2024; Accepted 5 August 2024
Available online 9 August 2024

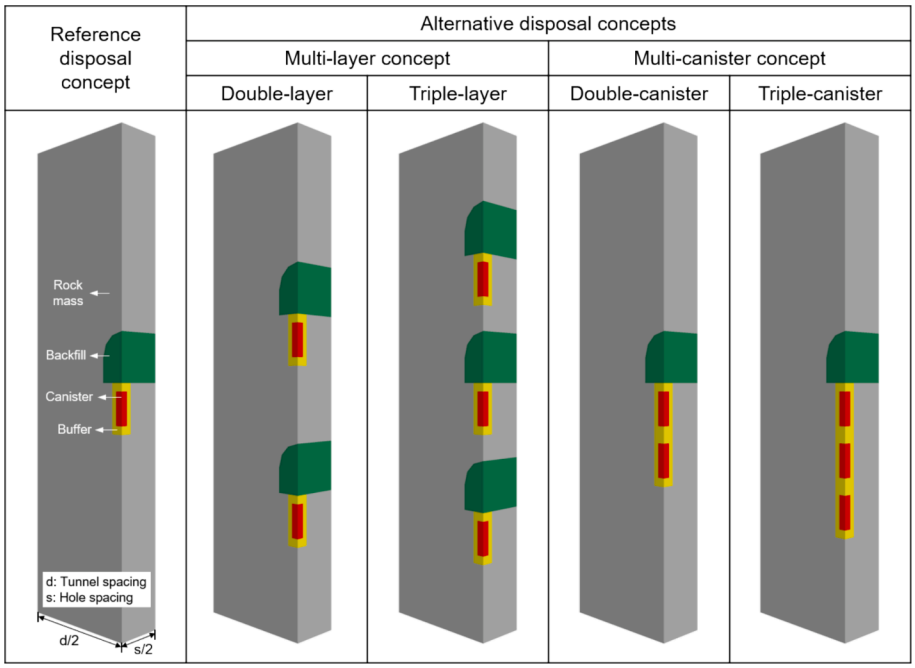

Fig. 1. Conceptual diagrams of a quarter section of a symmetrical disposal module for reference and alternative disposal concepts. *d* and *s* denote disposal tunnel spacing and deposition hole spacing, respectively.

deposition holes containing SNFs (Zheng et al., 2015). However, a considerably large area required for the DGR designed with a thermal limit of 100 °C can cause difficulties in finding a suitable site, particularly in highly populated countries with limited land areas (Cho and Kim, 2016; Lee et al., 2020a; Lee et al., 2023b). This necessitates the development of alternative DGRs with reduced disposal areas for effective use of national territory and mitigation of social acceptance issues. Numerous laboratory and numerical studies have assessed the performance of bentonite at temperature exceeding 100 °C to adjust the thermal design constraint (Yoon et al., 2022; Cho and Kim, 2016, Wersin et al., 2007; Zheng et al., 2015; Couture, 1985). Although physical phenomena related to the long-term stability of the repository above 100 °C have not been fully understood yet, partially due to complex multiphase fluid flow and heat processes (Chang et al., 2022), various studies suggest that changes in the swelling performance of bentonite, which affect the integrity of the repository, are not significant around 125 °C (Cho and Kim, 2016; Wersin et al., 2007; Pusch et al., 2003). In that context, National Cooperative for the Disposal of Radioactive Waste (NAGRA) in Switzerland adopted 125 °C as the thermal limit of the buffer, measured at the outer half of the bentonite barrier for their repository design and layout (NAGRA, 2002). Efforts to demonstrate the performance of bentonite at high temperatures under realistic conditions have been undertaken through several field experiments involving different types of host rocks (Bossart et al., 2017; NAGRA, 2019; Kober et al., 2023). In-situ heater tests, aiming to investigate key coupled thermo-hydro-mechanical (THM) processes and parameters of EBS materials, named HE-E and FE (Full-scale emplacement) experiments, were conducted at the Mont Terri underground research laboratory located in the Opalinus clay formation in Switzerland (Bossart et al., 2017; NAGRA, 2019). The temperature at the interface between the buffer and heater was increased by more than 130 °C. For granitic host rocks, an international field experiment titled "High Temperature Effects on Bentonite Buffers (HotBENT)" was initiated at the Grimsel test site in Switzerland (Kober et al., 2023). The heating of two types of bentonites, namely Wyoming-type bentonite and Czech bentonite of type BCV (Bentonite Černý Vrch), up to 200 °C commenced in 2021 in two sectors separated by cement-based plugs. These sectors are scheduled to be dismantled after 5 and 20 years of heating, respectively (Kober et al., 2023).

Development of alternative disposal concepts including multi-layer and multi-canister repositories (Fig. 1) has been considered as an additional option to reduce repository area in several countries (Kwon and Choi, 2006; Cho et al., 2017; Lee et al., 2020a; Malmlund et al., 2004; Carvalho and Steed, 2012). In Korea, Kwon and Choi (2006) evaluated thermal performance and rock mass stability of the multi-layer concept using thermo-mechanical numerical simulations. Cho et al. (2017) assessed the multi-layer and multi-canister repositories in terms of temperature, mechanical stability, and nuclear criticality, demonstrating a disposal density improvement of 200 % to 400 % compared to the single-layer repository. Lee et al. (2020a) conducted numerical analysis on coupled THM behavior in single- and multi-layer repositories based on the Korean reference disposal system (KRS). The double-layer disposal concept was considered as an alternative layout for a DGR at Olkiluoto in Finland with an approximately 20 % smaller area than the single-layer disposal concept (Malmlund et al., 2004). In Canada, Carvalho and Steed (2012) calculated optimized disposal spacing in the double-layer concept and investigated ground uplift and rock failure using thermo-mechanical analysis.

The disposal area can also be reduced through the optimization of decay heat per canister. Jeong et al (2022) developed a computer program called ACom (Assembly Combination), by which respective SNFs with maximum and minimum decay heat are iteratively placed in a canister. The optimum combinations of SNFs per canister calculated by ACom resulted in relatively lower decay heat compared to a conventional model assuming that all SNFs in a canister emits identical decay heat (hereafter referred to as the reference decay heat model). Based on the optimized decay heat model derived by Acom, along with an increased thermal limit of the buffer, Lee et al. (2023b) proposed a high-efficiency DGR, significantly reducing the disposal area by 40 ~ 60 % compared to an existing disposal system in Korea, but the multi-layer concept was not considered in their study.

In order to provides various options for designing a high-efficiency DGR tailored to the target disposal area and rock mass qualities in potential repository sites, this study presents a numerical investigation for the enhancement of disposal efficiency, which is inversely proportional to the total disposal area, incorporating three design factors for DGRs:

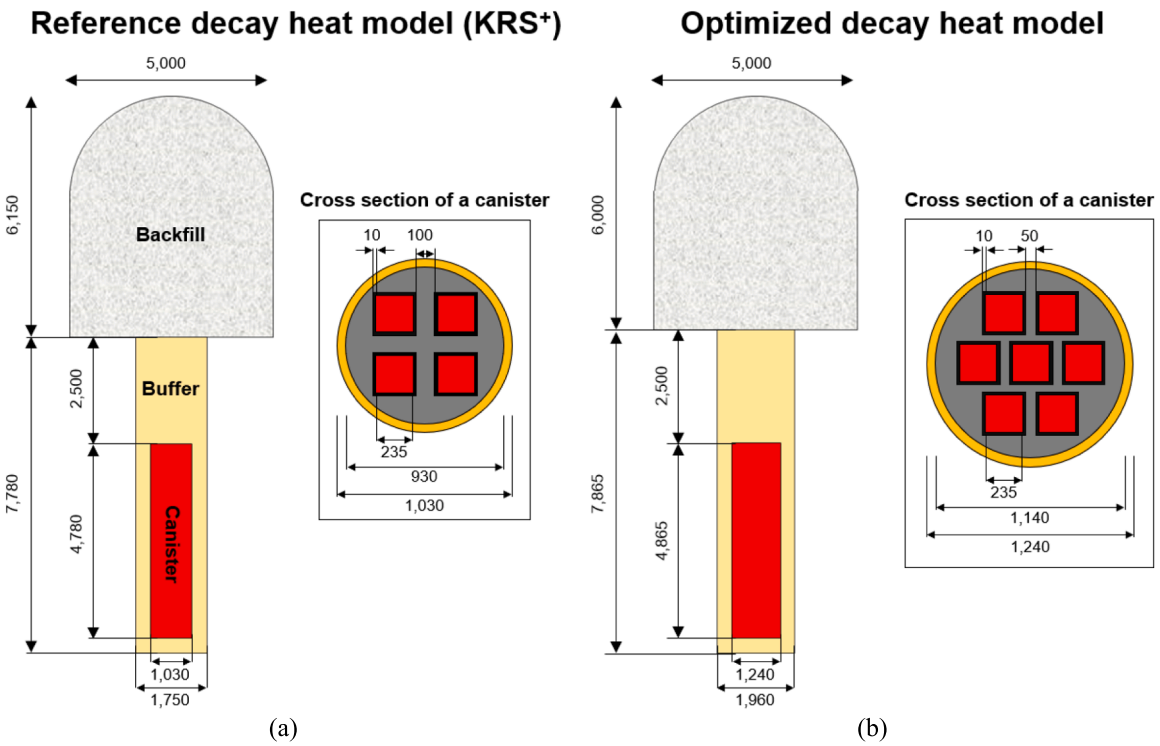

Fig. 2. Unit disposal modules and cross sections of canisters for (a) the reference (modified from Lee et al. (2020b)) and (b) optimized (modified from Lee et al. (2023b)) decay heat models.

decay heat optimization, increased thermal limit of the buffer, and double-layer concept. Specifically, an existing disposal concept in Korea designed with the reference decay heat model and termed the improved Korean reference disposal system (KRS^{+}) is used as a reference DGR with brief introduction in the next section (Section 2). Section 2 also provides descriptions of the optimized decay heat model. The numerical model setup including simulation cases, model geometry, initial and boundary conditions, and model properties is presented in Section 3. Section 4 presents simulation results such as comparison of repository performances with the reference and optimized decay heat models, determination of optimal disposal spacings considering the three design factors, mechanical stability of the host rock, and the effect of layer spacing in the double-layer concept. Discussions on the effect of material properties and rock mass stability issues in both near- and far-fields are provided in Section 5, followed by the conclusion in Section 6.

2. Reference and optimized decay heat models

In Korea, a series of disposal concepts were developed based on a thermal limit of the buffer of 100 °C. Initially, the Korean reference disposal system (KRS) was introduced by Korea Atomic Energy Research Institute (KAERI) (Lee et al., 2007) referring to the KBS-3 V concept designed by the Swedish Nuclear Fuel and Waste Management Company (SKB) (SKB, 2010). For pressurized water reactor (PWR) SNFs with an initial enrichment of 4.0 wt% and a discharged burn-up of 45 GWd/MtU corresponding to the initial decay heat per canister of 1.915 kW, the spacings of disposal tunnel and deposition hole for KRS were 40 m and 6 m, respectively. In 2013, KRS-HB was developed for high burn-up SNFs with an initial enrichment of 4.5 wt% and a discharged burn-up of 55 GWd/MtU, featuring spacings of 40 m for disposal tunnel and 9 m for deposition hole (Kim et al., 2013). The improved Korean reference disposal system (KRS^{+}) is the up-to-date concept that enhances disposal

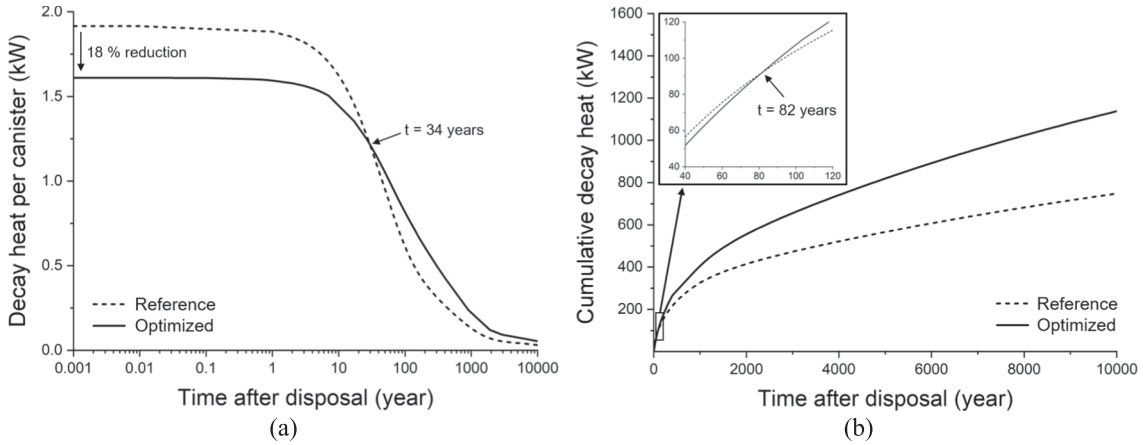

Fig. 3. Variations of (a) the decay heat per canister and (b) cumulative decay heat for the reference and optimized decay heat models.

efficiency through modifications to the dimensions and cooling time of the SNFs (Lee et al., 2020b). The deposition hole spacing for KRS$^+$ was reduced to 7.5 m, while the disposal tunnel spacing was maintained.

Detailed strategies for optimizing decay heat per canister are provided in Lee et al. (2023b). Descriptions of the optimized decay heat model are briefly presented in this study in comparison with the reference decay heat model used for the KRS$^+$. Fig. 2 shows unit disposal modules and cross sections of canisters for the reference and optimized decay heat models. In the KRS$^+$, four reference SNFs releasing identical decay heat are placed in a canister with an assumed cooling time of 45 years (Lee et al., 2020b). For the optimized decay heat model, seven SNFs with maximum and minimum decay heat depending on actual burn-up and cooling time are iteratively combined in a canister using the ACom program (Jeong et al., 2022). Consequently, the decay heat of each canister is evenly distributed with a relatively low level of maximum decay heat at the beginning compared to the reference decay heat model (Jeong et al., 2022). The average cooling time of SNFs in the canister of the optimized decay heat model is 93 years if the operation of the repository is initiated from 2070. The diameters of the canister and deposition hole in the optimized model are increased from those of the KRS$^+$ to contain three additional SNFs. The radial thickness of the buffer between the canister and the wall of the deposition hole is maintained as 36 cm. Fig. 3a shows the variations of decay heat per canister for the reference and optimized decay heat models after disposal. The initial decay heat of the optimized decay heat model is 1.563 kW, which is 18 % lower than that of the reference decay heat model, but both are reversed about 34 years after disposal (Fig. 3a). Fig. 3b shows the cumulative decay heat for both models, indicating the total emitted thermal energy from the canister. The cumulative decay heat of the optimized model exceeds that of the reference decay heat model about 82 years after disposal, and the total decay heat released from the optimized decay heat model is approximately 52 % larger than that from the reference decay heat model 10,000 years after disposal.

3. Numerical model setup

3.1. Numerical simulator and coupling procedure

A numerical simulator employed in this study is the TOUGH2-MP/FLAC3D simulator, which couples the two commercial codes: TOUGH2-MP (Zhang et al., 2008) and FLAC3D (Itasca, 2012). TOUGH2-MP is a parallel version of TOUGH2 (Pruess et al., 1999) used for modeling multiphase and multicomponent fluid flow and heat transfer. FLAC3D is employed for handling coupled thermo-hydro-mechanical processes in rock and soil mechanics. The TOUGH-FLAC simulators (Rutqvist et al., 2002; Rutqvist, 2017; Rinaldi et al., 2022) linking the TOUGH-family codes such as TOUGH2 and TOUGH3 with various versions of FLAC3D has been widely applied in various applications related to coupled THM processes in the subsurface such as oil and gas development (Rutqvist et al., 2013), CO_2 geosequestration (Rutqvist and Tsang, 2002; Rinaldi et al., 2022), enhanced geothermal systems (Jeanne et al., 2014; Kim et al., 2022a), and deep geological disposal (Rutqvist et al., 2014; Tounsi et al., 2023). The TOUGH2-MP/FLAC3D simulator uses a similar but faster calculation algorithm compared to the original TOUGH2 and FLAC3D version by means of parallel computing systems, so it was mainly applied to the long-term performance evaluation of the DGRs (Lee et al., 2020a; Lee et al., 2021; Kim et al., 2021).

Detailed coupling procedures of the TOUGH-FLAC simulator almost identical to those of the TOUGH2-MP/FLAC simulator are presented in Rutqvist et al. (2002), and are briefly summarized here. The coupled equations in TOUGH2-MP and FLAC3D are solved sequentially by exchanging coupling parameters at specific time intervals. Pressure, temperature, and saturation data calculated after solving the thermal–hydraulic equations in TOUGH2-MP on the Linux operating system are transferred to FLAC3D via a coupling algorithm embedded in TOUGH2-MP. Subsequently, the mechanical equations in FLAC3D are solved considering the pore pressure, swelling stress, and thermal stress to update the stress and strain of the medium. TOUGH2 then solves the thermal–hydraulic equations with the updated permeability and porosity based on the stress and strain data transferred from FLAC3D. In this study, however, we uses a partially-coupled scheme, in which the mechanical effect on thermal and hydraulic conditions are not considered.

3.2. Governing equations

The basic mass and energy balance equations solved by TOUGH2-MP are as follows:

$$\frac{d}{dt}M^\kappa + \nabla \bullet \boldsymbol{F}^\kappa = q^\kappa \tag{1}$$

where t is time M is total mass or energy, κ is the mass or heat component (water and air), F is mass or heat flux, and q is the sink or source.

The general form of the mass accumulation term is obtained by summing over the fluid phase β as given in Eq. (2).

$$M^\kappa = \phi \sum_\beta S_\beta \rho_\beta X_\beta^\kappa \tag{2}$$

where ϕ is the porosity, S_β and ρ_β are the saturation and density of phase β, respectively, and X_β^κ is the mass fraction of component κ present in phase β.

The heat accumulation term in a multiphase system is

$$M^K = (1-\phi)\rho_R C_R T + \phi \sum_\beta S_\beta \rho_\beta u_\beta \tag{3}$$

where ρ_R and C_R are the grain density and specific heat of the rock, respectively, T is the temperature, and u_β is the specific internal energy in phase β.

Advective mass flux is a sum over phases, and individual phase fluxes are given by a multiphase version of Darcy's law:

$$F_{adv}^\kappa = \sum_\beta X_\beta^\kappa \boldsymbol{F}_\beta = \sum_\beta X_\beta^\kappa \rho_\beta \boldsymbol{u}_\beta = \sum_\beta X_\beta^\kappa \left(-k \frac{k_{r\beta}\rho_\beta}{\mu_\beta}\left(\nabla P_\beta - \rho_\beta \boldsymbol{g}\right)\right) \tag{4}$$

where $\boldsymbol{u}_\beta$ is the Darcy velocity in phase β, k is the absolute permeability, $k_{r\beta}$ is the relative permeability to phase β, μ_β is the viscosity, P_β is the fluid pressure in phaseβ, and $\boldsymbol{g}$ is the vector of gravitational acceleration.

Along with the Darcy flow, the diffusive mass transport is

$$F_{diff}^\kappa = -\sum_\beta \phi \tau_0 \tau_\beta \rho_\beta d_\beta^\kappa \nabla X_\beta^\kappa \tag{5}$$

where $\tau_0\tau_\beta$ is the tortuosity, defined as a product of a porous medium dependent factor, τ_0 and a coefficient depending on phase saturation, τ_β, and d_β^κ is the molecular diffusion coefficient for component κ in phaseβ.

Heat flux including conductive and convective components is

$$F^H = -\lambda \nabla T + \sum_\beta h_\beta F_\beta \tag{6}$$

where λ is the thermal conductivity and h_β is the specific enthalpy in phase β.

In the case of static equilibrium of the medium, the linear momentum equation solved by FLAC3D is as follows:

$$\nabla \bullet \boldsymbol{\sigma} + \rho \boldsymbol{b} = 0 \tag{7}$$

where $\boldsymbol{\sigma}$ is the Cauchy stress tensor, $\boldsymbol{b}$ is the vector of body forces.

The effective stress can be calculated as

$$\boldsymbol{\sigma}' = \boldsymbol{\sigma} - \boldsymbol{I}\alpha P \tag{8}$$

where $\boldsymbol{\sigma}'$ is the effective stress tensor, $\boldsymbol{I}$ is the unit tensor, P is the pore

Table 1
Decay heat model, thermal limit of the buffer and the number of layers for the reference and four alternative cases.

Case	Decay heat model	Thermal limit of the buffer (°C)	Number of layers
KRS^{+} (reference)	Reference	100	Single
OS100	Optimized	100	Single
OS130	Optimized	130	Single
OD100	Optimized	100	Double
OD130	Optimized	130	Double

pressure.

3.3. Simulation cases

Five simulation cases are generated to investigate the increase in disposal efficiency based on the three design factors of the DGR: decay heat model, thermal limit of the buffer and the number of layers (Table 1). The first case is the reference case representing the conditions of the KRS^{+} with the reference decay heat model, a thermal limit buffer of 100 °C and the single-layer concept. Other four cases are the alternative DGRs named after the used design factors. For example, the case named OS100 uses the optimized decay heat model (O), the single-layer

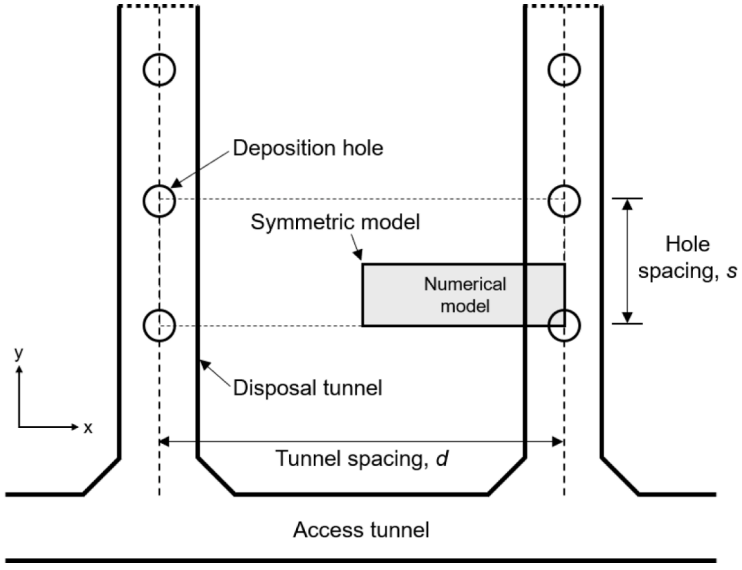

(a)

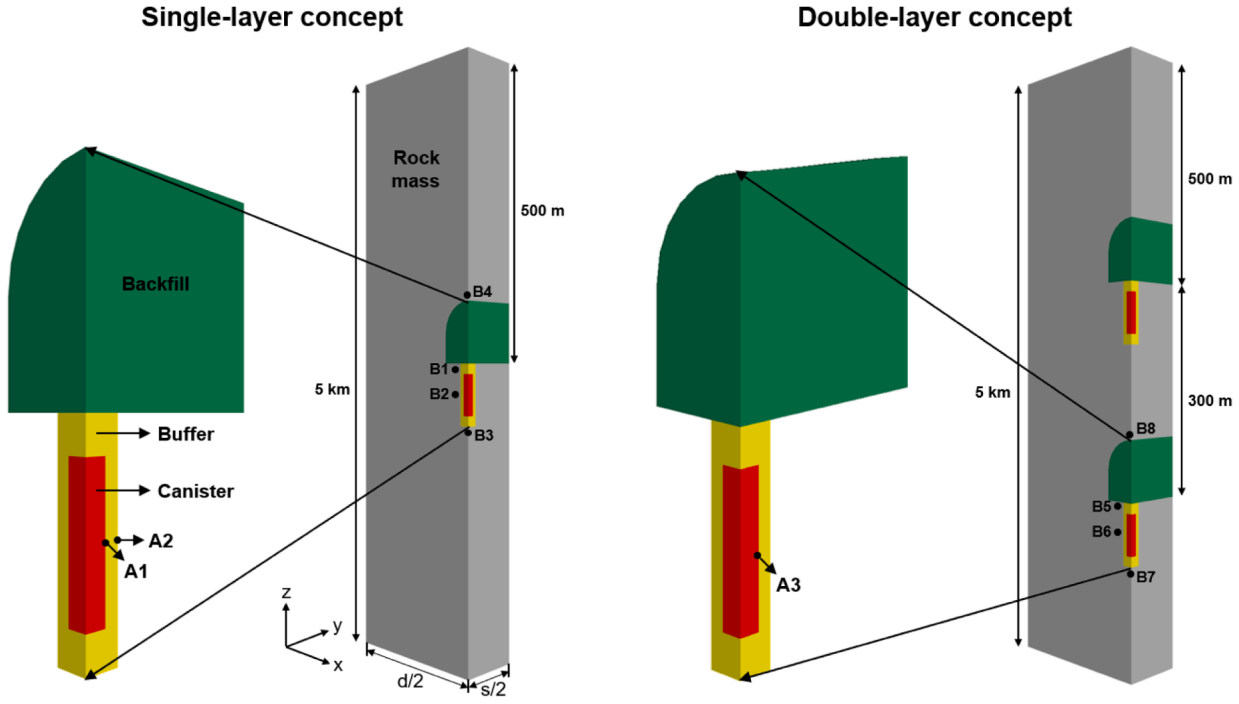

(b) (c)

Fig. 4. (a) Schematic diagram of the disposal tunnels and deposition holes from top-down view illustrating the periodicity of the symmetrical numerical model. Geometry of a quarter section of a symmetrical disposal module for the (b) single- and (c) double-layer concepts with data monitoring points at buffer (A1 to A3) and rock mass (B1 to B8) (not to scale). *d* and *s* indicate the spacings of disposal tunnel and deposition hole, respectively.

concept (S), and a thermal limit of the buffer of 100 °C (100). The effect of decay heat optimization on the enhancement of disposal efficiency can be identified by comparing the disposal area of the reference case and OS100. In addition to the decay heat optimization, increased thermal limit of the buffer to 130 °C and the double-layer concept are considered in OS130 and OD100, respectively. Lastly, OD130 takes advantage of all three design factors together, and the highest enhancement of disposal efficiency is expected.

3.4. Geometry and initial and boundary conditions

Considering the periodicity of the repository design with fixed disposal spacings, a quarter section of a symmetrical disposal module is generated for the single- and double-layer concepts with data monitoring points at the buffer and rock mass (Fig. 4). The quarter symmetric geometry represents simultaneous excavation of neighboring disposal tunnels and deposition holes, and heating of the disposal system. In the double-layer concept, data monitoring points are located at the lower layer, as the temperature of the buffer at the lower layer is higher than that at the upper layer due to the effect of the geothermal gradient. A1 to A3 are located in the buffer for calculating temperature, pressure, and saturation. Near-field rock mass stresses are calculated at B1 to B8. The sizes of the disposal tunnel and deposition hole refer to the geometry of the unit disposal modules shown in Fig. 2. The canister is assumed to be an equivalent single material emitting a quarter of the decay heat per canister given in Fig. 3. The height of the single- and double-layer models is set to 5 km to eliminate boundary effects from the fixed temperature at the bottom of the models. For the reference case, the spacings of disposal tunnel (d) and deposition hole (s) are 40 m and 7.5 m, respectively, which are identical to those of the KRS^{+}. For the four alternative cases, various values of the deposition hole spacings are used to identify the optimal disposal spacing satisfying the thermal limit of the buffer. The distance between the upper and bottom layers in the double-layer concept is arbitrarily fixed as 300 m.

No fluid flow and heat transfer occur at all lateral boundaries, indicating that the numerical domains are surrounded by identical decay heat sources, indicating the conditions at the center of a repository for the conservative analysis. The displacement normal to the lateral and bottom boundaries is fixed, whereas the free displacement condition is applied at the upper boundary, representing the ground surface. This boundary conditions were used in several previous studies, using the quarter symmetric repository models (Rutqvist et al., 2005; Lee et al., 2020a; Rutqvist, 2020). Temperature and pressure are fixed as 10 °C and 0.1 MPa, respectively at the ground surface. A geothermal gradient of 0.03 °C/m and a hydrostatic condition are considered in the remaining domain, excluding the EBS materials. The initial temperature and pressure of the EBS materials are set as 15 °C and 0.1 MPa, respectively considering the excavation and ventilation of the repository for 10 years. Initial liquid saturation of the EBS materials is set as 0.507 converted from an initial water content of 13 % according to Choi et al. (2008) except for a canister assumed to be in a dry condition. The in-situ stress condition is applied according to Eqs. (9)-(11) representing the regional stress in the Korean peninsula (Synn et al., 2013). Here, Z indicates the depth using a positive value, and the compressive stress is expressed by a positive value.

$$\sigma_x(MPa) = 0.0202Z + 1.5405 \tag{9}$$

$$\sigma_y(MPa) = 0.0352Z + 1.5759 \tag{10}$$

$$\sigma_z(MPa) = 0.0265Z \tag{11}$$

3.5. Model properties

The material properties of canister, buffer, backfill and rock mass listed in Table 2 are identical to those provided in Lee et al (2020a), which were used to model the coupled THM behaviors of the KRS and multi-layer disposal concepts. This study considers crystalline rock as a host rock for the DGR due to its low permeability, high strength, and stable geological conditions (Birkholzer et al., 2012; Kwon and Min, 2021). The rock properties were mostly measured by laboratory tests using granite specimens from the KAERI underground research tunnel (KURT) and the temperature (T)-dependent linear thermal expansion coefficient (α_T) is considered as Eq. (12) (Lee et al., 2019). Measured properties of the Ca-type bentonites produced in Korea, called KJ-I and KJ-II are used for the buffer (Lee and Cho, 2009; Lee et al., 2019; Yoon et al., 2018, Cho et al., 1999; Cho et al., 2010). Most of the properties of backfill and canister are assumed.

Table 2
The properties of EBS materials and rock mass used for the coupled THM modeling of the DGRs (Lee et al., 2020a).

Parameter (unit)	Canister	Buffer	Backfill	Rock mass
Density (kg/m^3)	6,577	1,600	1,600	2,650
Porosity (%)	0.001	41.0	40.0	1.16
Dry thermal conductivity (Wm^{-1}K^{-1})	401	0.521	1.00	3.05
Wet thermal conductivity (Wm^{-1}K^{-1})	401	1.234	2.00	3.31
Specific heat (Jkg^{-1}K^{-1})	390	1.061	980.0	820.0
Thermal expansion coefficient (°C^{-1})	1.7×10^{-5}	5.0×10^{-6}	5.0×10^{-6}	Eq. (12)
Permeability (m^2)	0.0	2.32×10^{-20}	1.0×10^{-19}	1.0×10^{-18}
van Genuchten's (1980) parameter, $1/P_{van}$ (MPa^{-1})	–	2.6×10^{-7}	3.3×10^{-7}	5.0×10^{-7}
van Genuchten's (1980) parameter, λ_{van} (–)	–	0.2941	0.5	0.6
Exponent for relative permeability, n	–	3.0	1.9	3.0
Residual liquid saturation (–)	0.01	0.01	0.01	0.01
Klinkenberg parameter (Pa^{-1})	–	5.0×10^{8}	1.61×10^{6}	6.86×10^{5}
Tortuosity (–)	–	0.67	0.80	0.80
Biot's coefficient (–)	–	1.0	1.0	1.0
Young's modulus (GPa)	155.0	0.59	0.59	32.8
Poisson's ratio	0.285	0.20	0.20	0.3
Maximum swelling stress (MPa)	–	5.0	3.0	–

$$\alpha_T = \left(0.7704\sqrt{T} + 1.3306\right) \times 10^{-6} \tag{12}$$

4. Simulation results

4.1. Repository performances using the reference and optimized decay heat models

Repository performances using the reference and optimized decay heat models are investigated under the condition that both models have identical disposal spacings for the KRS^{+} based on coupled TH simulations. Fig. 5 shows the thermal and hydraulic behaviors of the buffer adjacent to a canister and rock for the reference and optimized decay heat models. In case of the reference decay heat model, the buffer temperature reaches a peak value of 82.0 °C after 18 years at the interface between the buffer and canister (A1). The optimized decay heat model presents a relatively slower increase in buffer temperature at A1 compared to the reference decay heat model, attributed to the smaller initial decay heat of the optimized decay heat model, but both decay heat models are reversed at 33 years after disposal. The maximum buffer temperature of the optimized decay heat model is calculated as 81.6 °C after 179 years. Contrary to the reference decay heat model, where the buffer temperature immediately decreases after reaching the peak value, the optimized decay heat model shows a flat peak, maintaining the temperature above 81.0 °C for approximately 300 years. This characteristic of the flat peak temperature might occur in the specific

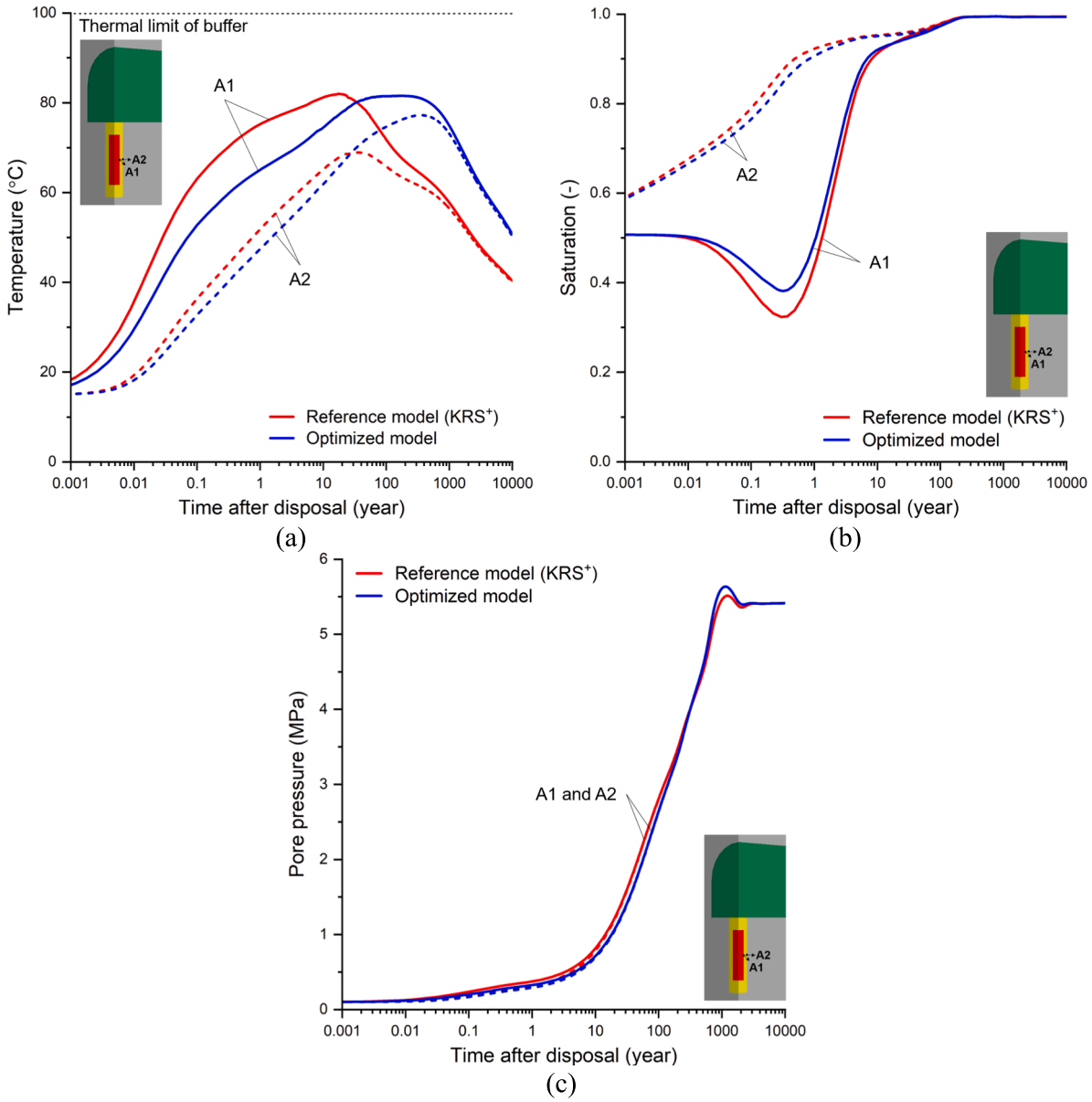

Fig. 5. Variations of the (a) temperature, (b) saturation, and (c) pressure at interfaces between the buffer and canister (A1) and between the buffer and rock mass (A2) for the reference and optimized decay heat models.

disposal spacings used here, where the relatively higher rate of heat accumulation in the buffer, caused by the larger decay heat of the optimized model after 34 years (Fig. 3a), is balanced with the rate of heat diffusion to the surrounding rock masses. The long-lasting peak temperature of the buffer in the optimized decay heat model can lead to a more evenly distributed temperature profile throughout the buffer compared to the reference decay heat model. Thus, the maximum temperature of the optimized decay heat model at the interface between the buffer and rock mass (A2) is calculated as 77.2 °C after 334 years, which is 8.3 °C higher and occurs 300 years later than that of the reference decay heat model.

The different thermal behavior of the reference and optimized decay heat models results in variations in hydraulic behavior at the buffer through coupled thermo-hydraulic processes. At the interface between the buffer and canister (A1), water evaporation initially occurs due to elevated temperature, causing a decrease in liquid saturation to a minimum of 0.32 and 0.38 for the reference and optimized decay heat models, respectively (Fig. 5b). The relatively rapid increase in temperature at the beginning period for the reference decay heat model induces more active vaporization in comparison with the optimized decay heat model. Increased suction at A1 due to reduced saturation draws water from the outer part of the buffer, causing continuous saturation increase, and the buffer is saturated more than 99 % after 170 years and 190 years for the reference and optimized decay heat models, respectively. At the interface between the buffer and rock mass (A2), groundwater flows from rock mass to the buffer due to suction and pressure difference, so the buffer is gradually saturated from the beginning and almost fully saturated after 167 years and 185 years for the reference and optimized decay heat models, respectively. In terms of the pore pressure evolution, both models are almost similar at A1 and A2, but the optimized decay heat model has slightly higher peak pore pressure possibly due to thermally-induced pore pressure increase (Fig. 5c).

Fig. 6 shows the temperature profiles along the vertical line passing through the center of the canister at different times for both models. Before disposal, the temperature distribution near the depth of the repository is lower than the temperature profile following the geothermal gradient owing to the excavation and ventilation effect (Fig. 6a). The temperatures of the reference and optimized decay heat models increase

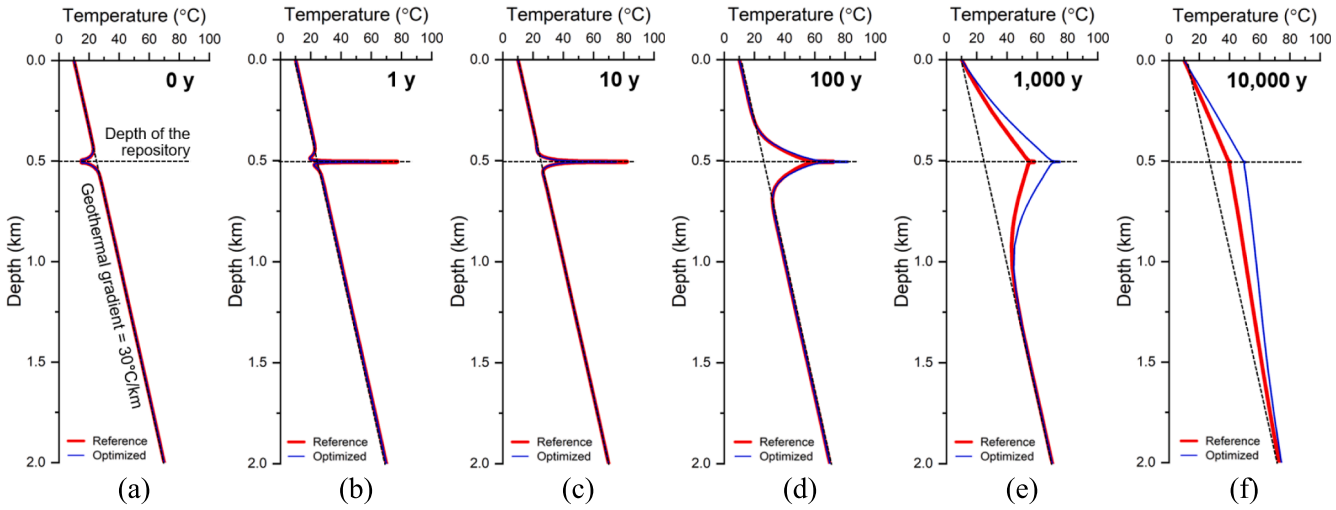

Fig. 6. Temperature profiles along the vertical line passing through the center of the canister at (a) 0, (b) 1, (c) 10, (d) 100, (e) 1,000 and (f) 10,000 years after disposal for the reference and optimized decay heat models.

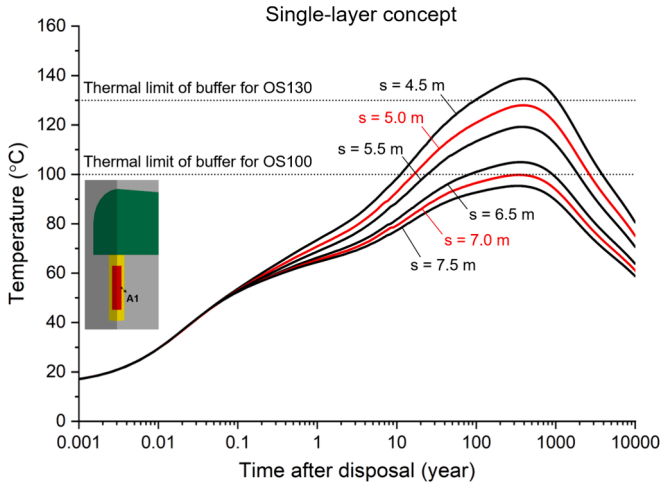

Fig. 7. Variations of buffer temperatures at A1 with various values of deposition hole spacings (s) for the single-layer concept. The optimized deposition hole spacings for the OS100 and OS130 are indicated by red lines. (For interpretation of the references to colour in this figure legend, the reader is referred to the web version of this article.)

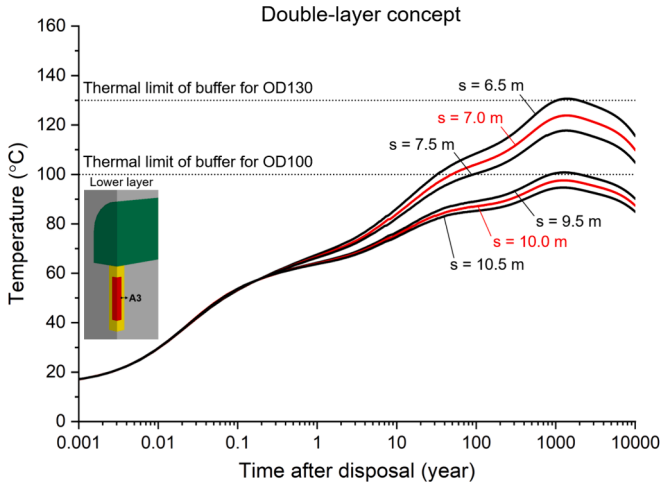

Fig. 8. Variations of buffer temperatures at A3 with various values of deposition hole spacings (s) for the double-layer concept. The optimized deposition hole spacings for the OD100 and OD130 are indicated by red lines. (For interpretation of the references to colour in this figure legend, the reader is referred to the web version of this article.)

to 77.2 °C and 66.5 °C, respectively near the depth of 500 m at one year after disposal, while the ventilation effect still remains in surrounding areas (Fig. 6b). The ventilation effect is eliminated in all areas at 10 years for both models, and the areas of elevated temperature continuously extend by the diffusion of decay heat to the upper and lower rock masses as time passes (c-6f). At 100 years, the spatial range and amount of temperature increase are similar for both models, but a larger amount of heat is accumulated throughout the rock mass for the optimized decay heat model as it emits a larger amount of cumulative decay heat per canister compared to the reference decay heat model. At 10,000 years, a temperature increase of 10 °C reaches approximately 1,000 m below the repository for the optimized decay heat model. Based on a simple calculation using Eq. (13), a temperature increase of 10 °C possibly induces thermal stress at the rock mass on the order of 10^{-1} MPa, which might trigger shear activation of critically-stressed existing fractures and faults (Reasenberg and Simpson, 1992; Stein, 1999).

$$\sigma_T = 3\alpha_T K \Delta T \tag{13}$$

where σ_T is the thermal stress, K is the bulk modulus used as 27.3 MPa in this study, and ΔT is the temperature change.

As undesirable permeability increase by fracture shear activation could degrade the safety performance of a DGR in terms of radionuclide transfer, a more in-depth analysis for the mechanical stability of the rock mass in far-field as well as near-field is required for the optimized decay heat model.

4.2. Estimation of the disposal spacings

In order to estimate the optimal disposal spacings of the four alternative DGRs in Table 1, satisfying the thermal limit of the buffer, numerous symmetrical disposal modules are generated with various values of deposition hole spacings. The interval between deposition hole spacings is set as 0.5 m, and the disposal tunnel spacing is fixed as 30 m for simplification. Variations of buffer temperature at A1 and A3, which represent the midpoint of the interface between the buffer and canister and the location of the largest temperature increase as calculated in previous studies (Lee et al., 2020a; Kim et al., 2021), are evaluated for the single-layer (OS100 and OS130) and double-layer (OD100 and

Table 3
The maximum buffer temperature, spacings of disposal tunnel and deposition hole, unit disposal area, and normalized disposal efficiency by the KRS$^+$ for the reference and alternative DGR cases.

Case	Maximum buffer temperature (°C)	Disposal tunnel spacing (m)	Deposition hole spacing (m)	Unit disposal area (m^2)	Normalized disposal efficiency (%)
KRS$^+$	82.0	40.0	7.5	75.0	1.0
OS100	99.8	30.0	7.0	30.0	2.5
OS130	128.0	30.0	5.0	21.4	3.5
OD100	97.6	30.0	10.0	21.4	3.5
OD130	123.9	30.0	7.0	15.0	5.0

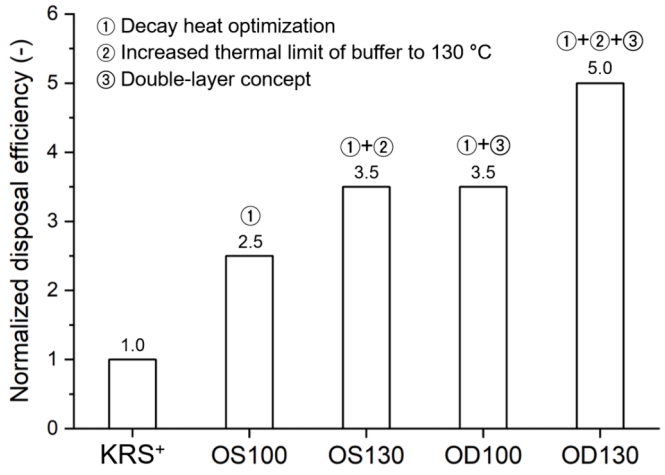

Fig. 9. Bar charts of the normalized disposal efficiency by the KRS$^+$ for the reference and alternative DGRs.

OD130) concepts through coupled TH simulations.

Figs. 7 and 8 present the variations of buffer temperature for the alternative DGRs in single- and double-layer concepts, respectively with various values of deposition hole spacings. In the cases of the single-layer concepts (Fig. 7), the evolution of buffer temperature is almost identical regardless of the deposition hole spacings in the very early periods before 0.05 years. Afterwards, DGRs with smaller deposition hole spacings result in more substantial temperature increases at the buffer, showing the peak temperature at a similar time, approximately between 300 and 400 years after disposal. The maximum buffer temperatures are calculated as 105.0 °C, 99.8 °C, and 95.3 °C for deposition hole spacings of 6.5 m, 7.0 m, and 7.5 m, respectively. Consequently, 7.0 m is determined as the optimal deposition hole spacing for OS100, conforming to the thermal limit of the buffer. In the same manner, the optimal deposition hole spacing for OS130 is identified as 5.0 m. In cases of the double-layer concepts (Fig. 8), one additional inflection point appears in the temperature evolution curves due to thermal interference caused by delayed heat transfer from the upper layer. Delayed thermal interference affects both the magnitude and timing of the peak temperature. For example, in the case of the deposition hole spacing of 7.5 m, the maximum buffer temperature is calculated as 117. 8 °C at approximately 1,350 years after disposal, which is 21.7 °C higher and 1,000 years later than the single-layer model with an identical deposition hole spacing. Relatively higher surrounding rock mass temperature at the lower layer due to the geothermal gradient could contribute to the larger temperature increase in the double-layer concepts. The optimal deposition hole spacings for OD100 and OD130 are determined as 10.0 m and 7.0 m, respectively. The maximum buffer temperatures and determined disposal spacings for the four alternative DGRs are presented in Table 3.

Based on the determined disposal spacings, the number of SNFs per canister and layers, unit disposal areas (A) for the four alternative DGRs are calculated using Eq. (14), where D is the disposal tunnel spacing, S is the deposition hole spacing, N is the number of SNFs per canister, and L is the number of layers. Disposal efficiencies of the reference and four alternative DGRs are calculated as the multiplicative inverse of the unit disposal area. These values are then normalized by the KRS$^+$. The unit disposal areas and normalized disposal efficiencies for the reference and four alternative DGRs are presented in Table 3.

$$A = \frac{DS}{NL} \tag{14}$$

Fig. 9 presents the normalized disposal efficiency with the used repository design factors for the alternative DGRs. By adopting the optimized decay heat model (OS100), the disposal efficiency can be increased as much as 2.5 times that of the KRS$^+$. In addition to the decay heat optimization, increasing the thermal limit of the buffer to 130 °C (OS130) or adopting the double-layer concept (OD100) provides an extra 40 % improvement in disposal efficiency. If all three design factors are applied together (OD130), the disposal efficiency can be enhanced to five times compared to that of the KRS$^+$, which could significantly alleviate the difficulties of site selection for the DGR, particularly related to the public acceptance issues. It should be carefully noted that this study solely uses the thermal limit of the buffer as a design constraint to determine the disposal spacings of the alternative DGRs. The determined disposal spacings can be modified if additional design constraints such as rock mass stability and performance degradation of EBS materials at high temperature are considered. Furthermore, securing a larger volume of continuous and homogeneous host rock in vertical direction for the double-layer concept may be more challenging from engineering and geological perspectives compared to the single-layer concept. However, this study merely assumes that such continuous and homogeneous vertical host rock can be secured for the potential DGR site.

4.3. Rock mass stability analysis

In the deep geological repository, temperature increase caused by decay heat under the confined conditions of the rock mass induces thermal stress (Rutqvist, 2000; Rutqvist and Tsang, 2004). Simultaneously, groundwater inflow from the surrounding rock alters the degree of saturation and pore pressure, resulting in the swelling of expansive buffer materials. The thermal stress and swelling stress can perturb the stress state in the repository, with a much larger stress perturbation applied to the rock mass compared to the buffer and backfill due to the relatively higher brittleness of the rock mass. Additional coupled THM simulations are conducted for the four alternative DGRs with the determined disposal spacings to analyze the mechanical stability of the rock mass based on two failure criteria. Firstly, the maximum effective principal stresses are compared to the half of the uniaxial compressive strength (UCS) of an intact rock to investigate potential spalling failure near the disposal tunnels and deposition holes (Martin, 2005). Since disposal tunnels and deposition holes are supported by swelling pressure from the buffer and backfill, considering the possibility of spalling failure of rock under the unconfined condition is a conservative approach (Lee et al., 2020a). Mohr-Coulomb failure criterion (Jaeger and Cook, 1979) is used as the second failure criterion to consider the enforced rock mass strength due to the confining stress generated by the swelling of buffer and backfill.

Fig. 10 shows variations in maximum principal stresses of the rock mass with the rock spalling failure criteria. As intact rocks have large variability in the UCS, ranging from less than a hundred to several hundred MPa (Chau and Wong, 1996; Zhao et al., 1999; Villeneuve et al., 2018), measured UCS values from granite specimens obtained at two different test locations in KURT are used for the spalling failure criteria. The average UCS values for granite specimens from the borehole heater (BH) test and in-situ demonstration of the engineered barrier system (In-DEBS) test are 91.4 MPa and 149.5 MPa, respectively (Lee

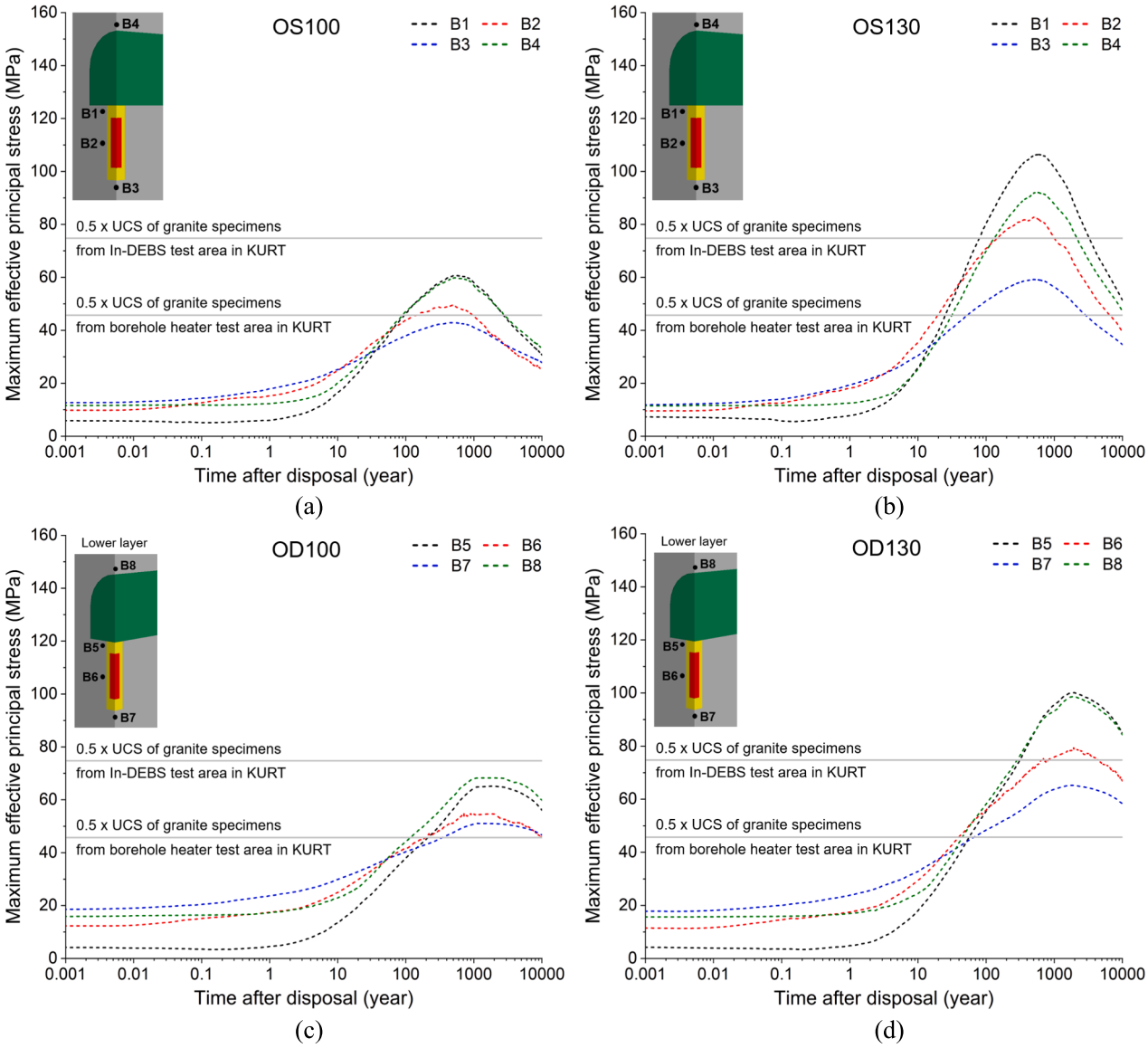

Fig. 10. Variations of the maximum principal stresses of rock mass near the disposal tunnel and the deposition hole for (a) OS100, (b) OS130, (c) OD100, and (d) OD130 with the failure criterion of rock spalling calculated as 50 % of the UCS of granite specimens from heater test and In-DEBS test areas in KURT.

et al., 2019). The overall trends in stress change for all alternative DGRs are similar to those of the temperature evolutions presented in Figs. 7 and 8 because the thermal stress is the primary cause of the rock stress change. Consequently, a broader area is anticipated to experience spalling failure in the cases with the thermal limit of 130 °C (OS130 and OD130) than the cases with the thermal limit of 100 °C (OS100 and OD100). For OS100 and OD100, spalling failure is expected at all monitoring points except at B3 of OS100 when the failure criterion based on the BH test is applied, whereas rock mass stability can be secured at all monitoring points when the failure criterion based on the In-DEBS test is applied. In contrast, for both OS130 and OD130, spalling failure can occur at all monitoring points except at the bottom of the deposition hole (B3 and B7), even with the failure criterion based on the In-DEBS test. It should be noted that the area of rock spalling failure might be overestimated, as the increase in rock mass strength due to confining stress by the swelling of buffer and backfill is not considered in this analysis.

Table 4
Empirical equations to calculate friction angle and cohesion of rock mass based on RMR (modified from Lee et al., 2020).

Property	Equation	Reference
Friction angle (°)	ϕ = -0.086 + 0.7891RMR-0.0031RMR^2	Bieniawski (1989)
	ϕ = 0.25RMR+27.5	Kim (1993)
	ϕ = 0.5RMR+5	Trueman (1988)
Cohesion (MPa)	C_o = 0.25exp(0.05RMR)	Trueman (1988)

The Mohr-Coulomb failure criterion describes the conditions for failure of an isotropic material with principal stresses (Eq. (15)), while the effect of the intermediate stress is excluded (Labuz and Zang, 2012).

$$\sigma_1 = \sigma_c + q\sigma_3 \tag{15}$$

where σ_c is the uniaxial compressive strength, and q is the slope between the minimum (σ_3) and maximum principal stresses (σ_1). σ_c and q can be calculated using cohesion (C_0) and friction angle (ϕ) as presented in Eqs. (16) and (17).

$$\sigma_c = 2C_0 cos\phi/(1 - sin\phi) \tag{16}$$

$$q = (1 + \sin\phi)/(1 - \sin\phi) \tag{17}$$

Table 5
Estimated values of mean friction angle (ϕ_m), cohesion (C_0), uniaxial compressive strength (σ_c) and slope between the minimum and maximum principal stresses (q) using the empirical equations listed in Table 4 for RMR of 60, 65, 70, 75, and 80.

Parameter	RMR				
	60	65	70	75	80
ϕ_m(°)	37.87	39.79	41.65	43.47	45.23
C_0 (MPa)	5.02	6.45	8.28	10.63	13.65
σ_c (MPa)	20.53	27.52	36.89	49.45	66.29
q (−)	4.18	4.55	4.96	5.41	5.90

Friction angle and cohesion of rock mass can be estimated based on rock mass rating (RMR) using empirical equations provided in Table 4. RMR is a geomechanical classification of rock mass quality into five classes: very poor (<20), poor (21 ~ 40), fair (41–60), good (61–80), very good (81–100) based on six parameters such as UCS, rock quality designation (RQD), spacing, condition, and orientation of discontinuities, and groundwater conditions (Bieniawski, 1989). The mean friction angle (ϕ_m) averaged from the three equations in Table 4, CO, σ_c and q are listed in Table 5 for various RMR values.

Fig. 11 presents the stress paths of the minimum and maximum effective principal stresses of rock mass at different times using the Mohr-Coulomb failure criteria. In all alternative DGRs, the intersection point of the disposal tunnel and deposition hole (B1 and B5) exhibits the most significant variation in the maximum effective principal stress due to high stress concentration, consistent with the findings of previous studies by Rutqvist et al. (2005) and Rutqvist and Tsang (2024). Conversely, the smallest variation in the minimum effective stress, which is the vertical stress, results from the relatively less vertically-confined condition caused by the low elastic modulus of the backfill as well as the tensional stress from swelling of the buffer in the vertical direction. This indicates minimized strengthening of rock mass strength. Thus, the intersection point of the disposal tunnel and deposition hole shows the highest susceptibility to failure among the monitoring points, necessitating an in-depth evaluation of rock mass failure and its impact

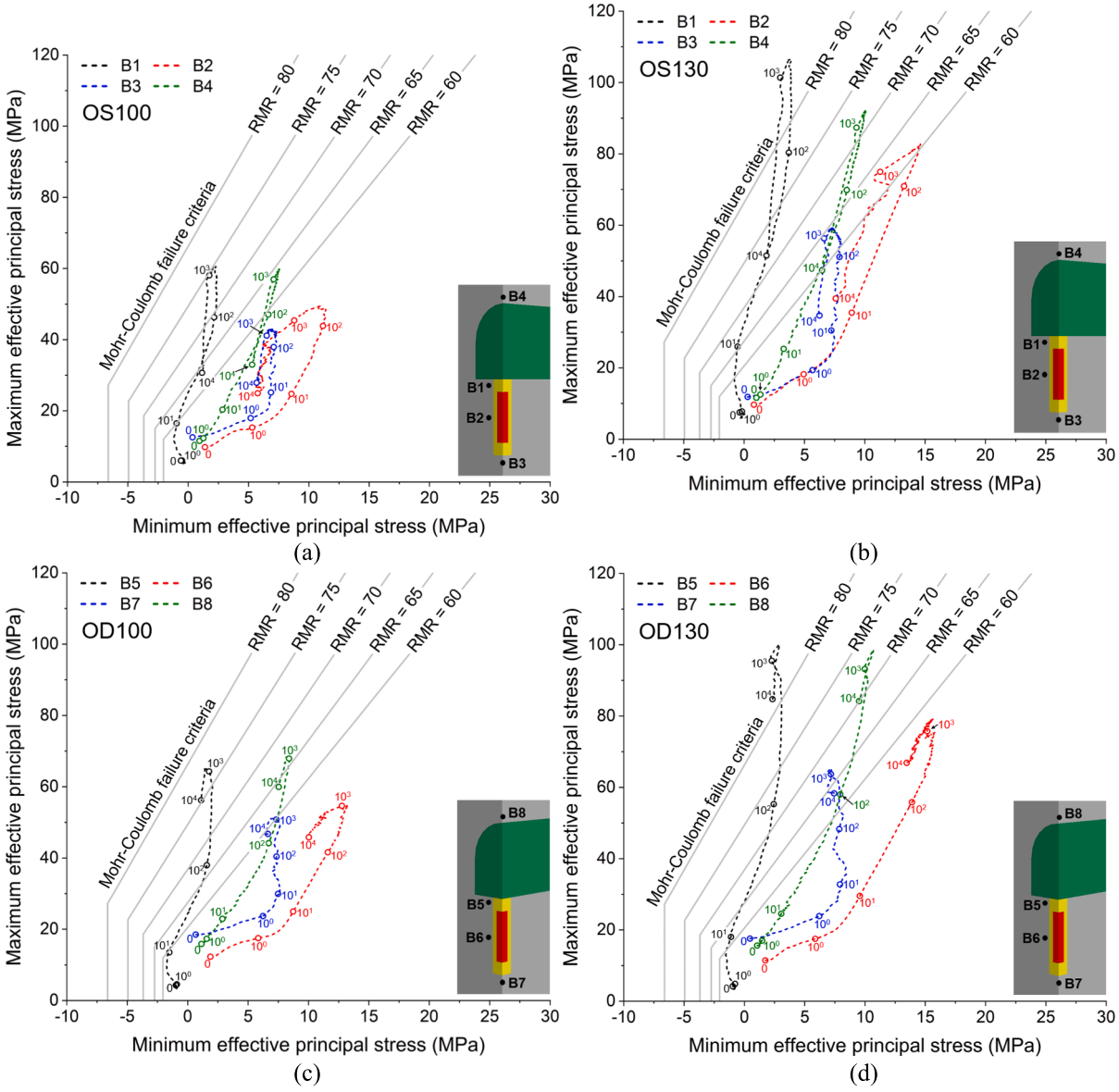

Fig. 11. Stress paths of the minimum and maximum effective principal stresses at the monitoring points of rock mass with the Mohr-Coulomb failure criteria for (a) OS100, (b) OS130, (c) OD100, and (d) OD130. The circles indicate the stress states at 0, 1, 10, 100, 1,000 and 10,000 years after disposal.

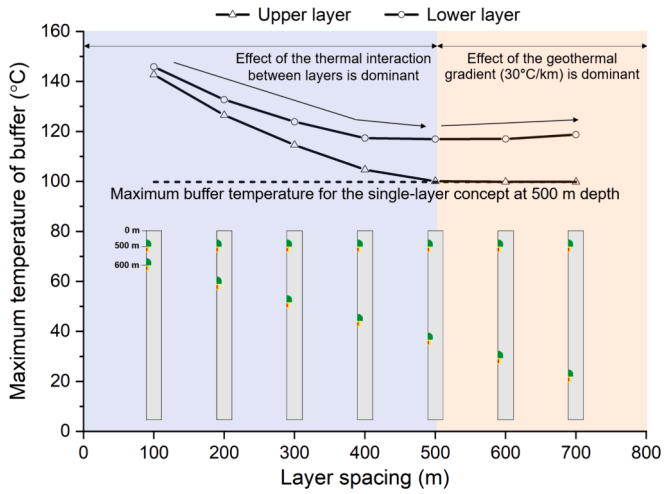

Fig. 12. Variations in the maximum buffer temperature at the upper and lower layers for OD130 under various layer spacings.

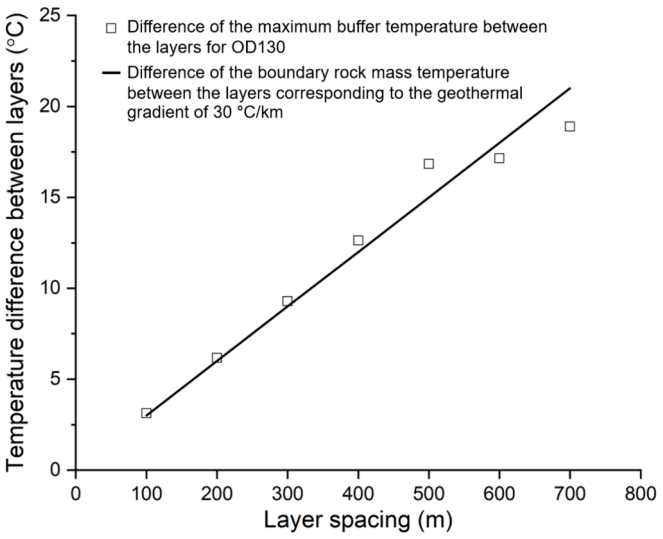

Fig. 13. The difference in both the maximum buffer temperature and the boundary rock mass temperature between the upper and lower layers for OD130 under various layer spacings.

on the EBS materials during the design of alternative DGRs.

On the other hand, the reinforced rock strength resulting from the largest increase in the minimum effective principal stress contributes to the reduced probability of failure at the rock mass in the vicinity of the center of the canister (B2 and B6). In the case of RMR of 60, corresponding to the highest rock mass quality categorized as 'fair', failure is anticipated at the intersection point of the disposal tunnel and deposition hole (B1 and B5) and the top of the disposal tunnel (B4 and B8) in all alternative DGRs. Except for OS100, the remaining three alternative DGRs also experience failure at the bottom of the deposition hole (B3 and B7). As RMR gradually increases from 60 to 80, the area susceptible to failure gradually decreases. In the case of RMR of 80, corresponding to the highest rock mass quality categorized as 'good', OS100 and OD100 exhibit no failure at any monitoring point. However, OS130 and OD130 still experience failure at the intersection point between the disposal tunnel and deposition hole due to the relatively high induced thermal stresses. According to RMR results investigated along a 252 m long declined borehole in KURT, approximately 63 % of the area exhibits RMR>60, and the area with RMR>80 is limited to only 24 % (Cho et al., 2013). Therefore, it is important to investigate the potential impact of the failure of the surrounding rock mass on the integrity of the EBS materials. In addition, increasing the thermal limit of the buffer may impose additional constraints on rock mass temperature.

4.4. *Effect of layer spacing*

In this study, the spacing between the upper and lower layers is assumed to be 300 m for the double-layer concept. However, the layer spacing can influence the buffer temperature due to the interplay between the boundary rock mass temperature and the thermal interaction between the upper and lower layers. Increasing the layer spacing weakens thermal interaction between the layers, reducing the maximum buffer temperature, while the higher boundary rock mass temperature at the lower layer influenced by the geothermal gradient inversely affects the maximum buffer temperature. In order to investigate the effect of layer spacing on the maximum buffer temperature, additional coupled TH simulations are conducted with various layer spacings for OD130. The layer spacing is increased from 100 m to 700 m, while the depth of the upper layer is fixed as 500 m.

Fig. 12 shows the variations in the maximum buffer temperature at the upper and lower layers with different layer spacings for OD130. At the upper layer, the maximum buffer temperature is calculated as 142.7 °C with a layer spacing of 100 m, and it decreases as the layer spacing increases. If the layer spacing exceeds 500 m, the effect of thermal interaction between the layers on the maximum buffer temperature nearly vanishes, as the maximum buffer temperature at the upper layer almost converges to the maximum buffer temperature at 500 m depth for the single-layer concept. At the lower layer, the maximum buffer temperature is higher than that at the upper layer due to the effect of the geothermal gradient. The difference in the maximum buffer temperature between the layers is similar to the difference in the boundary rock mass temperature between the layers, corresponding to the geothermal gradient of 30 °C/km (Fig. 13). The maximum buffer temperature at the lower layer declines as the layer spacing increases, and it has the lowest value as 116.9 °C when the layer spacing is 500 m. The maximum buffer temperature begins to rise with higher layer spacing due to the dominant effect of the geothermal gradient. If the layer spacing is set as 500 m, the disposal efficiency could be further enhanced in the double-layer concept. However, determine the optimal layer spacing requires engineering judgement, considering not only the thermal performance of the DGR but also various factors such as cost and difficulties of the construction as well as geomechanical conditions such as fluid pressure and in-situ stresses.

5. Discussion

This study provides a numerical investigation to enhance the disposal efficiency based on three design factors for a deep geological repository: decay heat optimization, increased thermal limit of the buffer, and the double-layer concept. Disposal spacings for the various alternative DGRs with different combinations of the design factors are determined using coupled TH simulations. Mechanical stability of near-field rock mass with different conditions of rock mass strength and qualities are identified through additional coupled THM simulations for the alternative DGRs with the determined disposal spacings. However, it is of importance to note that the calculated maximum buffer temperature and the determined disposal spacings in this study may vary depending on the type of SNFs and the properties of the buffer and rock mass. Numerous attempts have been made recently to improve the thermal conductivity of buffer materials with various additives (Rutqvist, 2020; Lee et al., 2023a; Feng et al., 2024), which enables more densely arranged canisters containing SNFs by means of the elevated heat release to surrounding rock masses. Kim et al. (2022b) developed regression equations estimating the peak buffer temperature based on various types of bentonite and rock thermal properties, offering disposal spacing maps for the Korean Peninsula. This highlights that

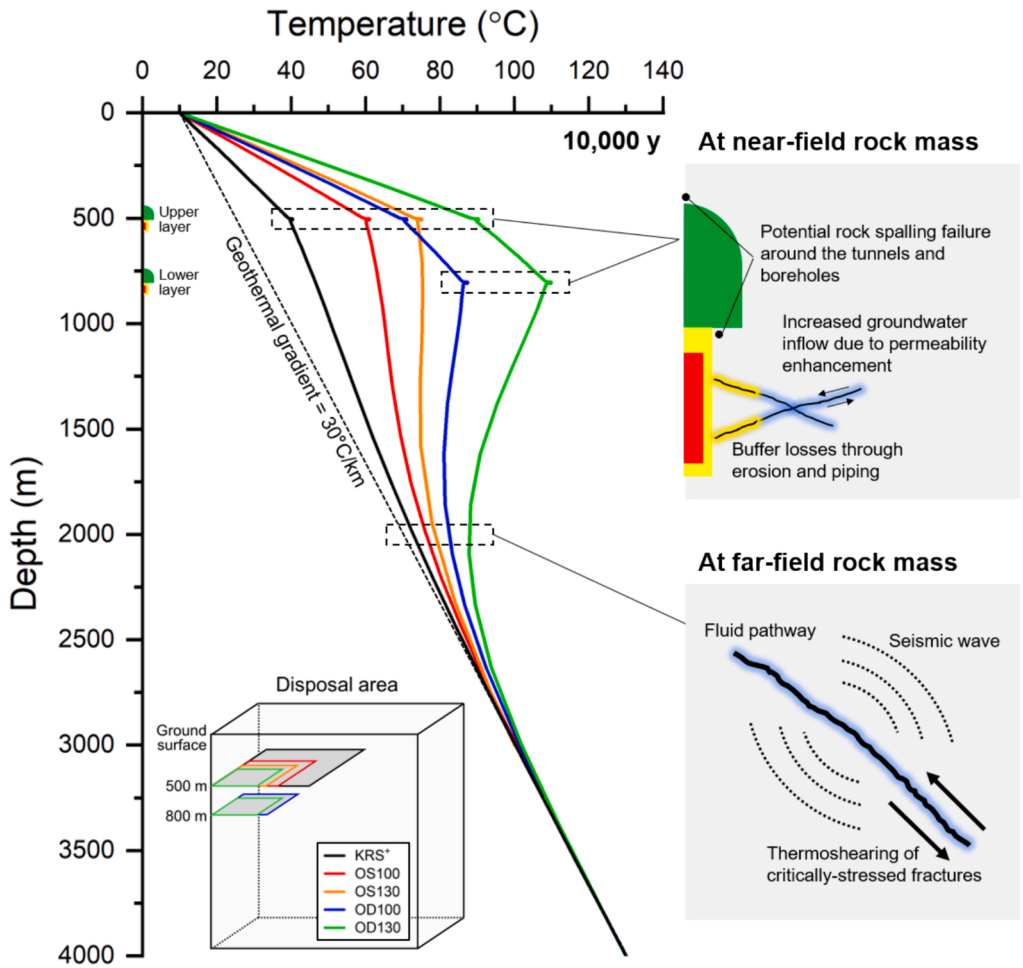

Fig. 14. Temperature profiles along the vertical line passing through the center of the canister at 10,000 years after disposal for the reference (KRS^{+}) and four alternative DGRs along with schematic diagrams showing a comparison of disposal areas and various phenomenon related to the possible thermally-induced failure in the near- and far-field host rock.

regional variations in rock properties can influence the disposal spacings. Thus, the disposal spacings for the alternative DGRs determined in this study should not be regarded as absolute values. Instead, emphasis should be placed on assessing the relative improvements in disposal efficiency compared to the reference DGR within the context of the specified type of SNFs and material properties.

The key outcome of this study is further illustrated in Fig. 14, which presents a comparison of disposal areas and temperature-depth profiles for the reference and four alternative DGRs together with schematic diagrams showing various phenomena related to the potential thermally-induced rock failure at near- and far-field scales. The combinations of three design factors can lead to a reduction in disposal areas from 20 % to 40 % of the current reference disposal system in Korea, which may substantially alleviate the difficulties associated with site selection for the DGR, particularly in gaining public acceptance. However, this study has a limitation in that the thermal limit of the buffer was used as a single design constraint to identify the disposal spacings without consideration of cost and difficulties of the construction as well as geomechanical aspects such as rock mass stability. Increasing the thermal limit of the buffer raises the probability of thermally-induced failure in the near-field host rock, resulting in irreversible permeability enhancement (Rutqvist and Stephansson, 2003; Min et al., 2005; Min et al., 2013). This, in turn, may lead to an increased groundwater inflow rate possibly degrading the integrity and performance of surrounding EBS materials through piping and erosion processes (Börgesson and Sandén, 2006; Suzuki et al., 2013). Thus, some deposition holes with high stress-strength ratio or large intersecting fractures, which are deemed susceptible to the thermo-mechanical damage, may be ruled out for the emplacement of SNFs. Moreover, an additional thermal constraint on rock mass may be imposed similar to a nuclear waste disposal concept in Switzerland, which allows a temperature up to 125 °C at half of the bentonite barrier with an additional thermal constraint on argillaceous host rock (Opalinus clay) of approximately 80 °C (Leupin et al., 2016; Rutqvist, 2020). The analysis of rock mass stability with various rock mass properties provided in this study (Figs. 10 and 11) can be briefly used to determine the suitability of deposition holes and the thermal constraint on granitic host rock. However, further studies are needed to investigate the extent of permeability increase and its impact on the performance of EBS materials. If the exclusion of certain deposition holes and the additional thermal constraint on rock mass are adopted into the design of alternative DGRs, the enhancement of disposal efficiency given in Fig. 9 might be reduced, particularly in cases with an increased thermal limit of the buffer.

Thermally driven fracture shear slip, termed as thermoshearing, in the far-field should be handled with importance as well, as it is associated with hydraulic and mechanical changes. These fractures serve as major pathways for fluid flow containing radionuclides (Min et al., 2005; Min et al., 2013). In addition, potential seismic events induced by fracture shear slip itself may raise public concern, similar to applications in enhanced geothermal systems and oil and gas development (Häring et al., 2008; Lei et al., 2013; Kim et al., 2022a). According to Seo et al.

(2024), who investigated shear slip potential around the reference and various alternative DGRs including multi-layer and multi-canister disposal concepts in the far-field scale, stress variations at distances several kilometers away were similar for the reference and alternative DGRs, as the total amount of SNFs corresponding to the total heat generation is the same for all DGRs. Nevertheless, the alternative DGRs with concentrated heat generation in relatively small areas exhibited higher stress variations compared to the reference DGR within a 1 km distance (see Fig. 6 in Seo et al., 2024). This study analogously identifies that more densely arranged heat sources for the alternative DGRs entail a larger temperature increase at the far-field scale (Fig. 14). However, studies on the potential fracture shear slip around the alternative DGRs are in an embryonic stage, and further in-depth investigations are needed, taking into consideration a network of discrete fractures, various in-situ conditions and rock types.

6. Conclusion

This study provides various options for designing a high-efficiency deep geological repository tailored to the target disposal area and rock mass qualities in potential repository sites. The key findings can be summarized as follows:

- The maximum buffer temperatures of the reference and optimized decay heat models are calculated as similar values. Contrary to the reference decay heat model, the buffer temperature of the optimized decay heat model exhibits a flat peak lasting about 300 years, resulting in a larger temperature increase in the rock mass at near- and far-field scales.
- Disposal efficiency can be increased as much as 2.5 times that of the current reference disposal system in Korea (KRS^{+}) solely by decay heat optimization (OS100). In addition to the decay heat optimization, increasing the thermal limit of the buffer to 130 °C (OS130) or adopting the double-layer concept (OD100) provides an extra 40 % improvement in disposal efficiency. If all three design factors are applied together (OD130), disposal area can be reduced by 20 % of that of the KRS^{+}, which may substantially alleviate the difficulties associated with site selection for the DGR.
- Deep geological repositories designed with an increased thermal limit of the buffer (OS130 and OD130) poses a greater probability of spalling failure in near-field host rock due to relatively high thermal stresses. Furthermore, rock mass failure can occur at the intersection point between the disposal tunnel and deposition hole for OS130 and OD130, based on the Mohr-Coulomb failure criterion derived from the assumed RMR of 80 regarded as the highest rock mass quality categorized as ‘good’.
- In the case of the double-layer concept, the maximum buffer temperature at the lower layer declines with increased layer spacing up to 500 m, because thermal interaction between the layers dominates over the effect of geothermal gradient. However, the maximum buffer temperature starts to rise with larger layer spacing because the thermal interaction between the layers almost disappears, and the boundary rock mass temperature increases following the geothermal gradient.

CRediT authorship contribution statement

Kwang-Il Kim: Writing – review & editing, Writing – original draft, Visualization, Methodology, Investigation, Formal analysis, Data curation, Conceptualization. **Changsoo Lee:** Writing – review & editing, Funding acquisition, Conceptualization. **Dongkeun Cho:** Funding acquisition. **Jonny Rutqvist:** Writing – review & editing.

Declaration of competing interest

The authors declare that they have no known competing financial interests or personal relationships that could have appeared to influence the work reported in this paper.

Data availability

Data will be made available on request.

Acknowledgements

This work was supported by the Innovative Technology Development Program for High-level waste management of the National Research Foundation of Korea (NRF) funded by the Korea government (Ministry of Science and ICT, MSIT) (Grant No.2021M2E3A2041312). This work was additionally supported by the Institute for Korea Spent Nuclear Fuel (iKSNF) and National Research Foundation of Korea (NRF) grant funded by the Korea government (Ministry of Science and ICT, MSIT) (2021M2E1A1085193). Additional funding was provided to J. Rutqvist by the U.S. Department of Energy under contract No. DE-AC0205CH11231 to the Lawrence Berkeley National Laboratory.

References

Ahonen, L., Korkeakoski, P., Tiljander, M., Kivikoski, H., Laaksonen, R., 2008. Quality assurance of the bentonite material, POSIVA Working Report 2008–33. Posiva Oy, Finland.
Bieniawski, Z.T., 1989. Engineering rock mass classifications. Wiley, New York.
Birkholzer, J., Houseworth, J., Tsang, C.F., 2012. Geologic disposal of high-level radioactive waste: Status, key issues, and trends. Annu. Rev. Env. Resour. 37, 79–106.
Börgesson, L. Sandén T., 2006. Piping and erosion in buffer and backfill materials. Current knowledge. SKB R-06-80. Swedish Nuclear Fuel and Waste Management Co., Sweden.
Bossart, P., Jaeggi, D., Nussbaum, C., 2017. Experiments on thermo-hydro-mechanical behaviour of Opalinus Clay at Mont Terri rock laboratory, Switzerland. J. Rock Mech. Geotech. Eng. 9, 502–510.
Carvalho, J.L., Steed, C.M., 2012. Thermo-mechanical analysis of a multi-level repository for used nuclear fuel. Nuclear Waste Management Organization, Canada. NWMO TR-2012-19,.
Chang, K.W., LaForce, T., Nole, M., Stein, E.R., 2022. Reduced-order THMC coupled simulation of nuclear waste disposal in shale. Proceedings of the 56th US Rock Mechanics/Geomechanics Symposium, Santa Fe, New Mexico, 26-29 June 2022. American Rock Mechanics Association ARMA, Paper No. 22-622.
Chau, K.T., Wong, R.H.C., 1996. Uniaxial compressive strength and point load strength. International Journal of Rock Mechanics and Mining Sciences & Geomechanics Abstracts 33 (2), 183–188.
Cho, W.J., Lee, J.O., Kwon, S., 2010. Analysis of thermo-hydro-mechanical behavior of the engineered barrier system of a high-level waste repository. KAERI/TR-4142/2010, Korea Atomic Energy Research Institute, Korea. (in Korean with English abstract).
Cho, W.J., Kim, G.Y., 2016. Reconsideration of thermal criteria for Korean spent fuel repository. Ann. Nucl. Energy 88, 73–82.
Cho, W.J., Kim, J.S., Lee, C., Choi, H.J., 2013. Gas permeability in the excavation damaged zone at KURT. Eng. Geol. 164, 222–229.
Cho, W.J., Lee, C., Kim, G.Y., 2017. Feasibility analysis of the multilayer and multicanister concepts for a geological spent fuel repository. Nucl. Technol. 200, 225–240.
Cho, W.J., Chun, K.S., Lee, J.O., 1999. Effect of dry density and temperature on the hydraulic conductivity of domestic compacted bentonite as a buffer material in the high-level waste repository. KAERI/TR-1223/1999, Korea Atomic Energy Research Institute, Korea. (in Korean with English abstract).
Choi, H.J., Lee, J.Y., Kim, S.S., Kim, S.K., Cho, D.G., Kim, K.Y., Jeong, J.T., Jeon K.S., 2008. Korean reference HLW disposal system. KAERI/TR-3563/2008, Korea Atomic Energy Research Institute, Korea. (in Korean with English abstract).
Couture, R.A., 1985. Steam rapidly reduces the swelling capacity of bentonite. Nature 318 (7), 50–52.
Feng, Y., Eun, J., Kim, S., Kim, Y.R., 2024. Evaluation of equivalent thermal conductivity for carbon fiber-reinforced bentonite through experimental and numerical analysis. Comput. Geotech. 165, 105880.
Häring, M.O., Schanz, U., Ladner, F., Dyer, B.C., 2008. Characterisation of the Basel 1 enhanced geothermal system. Geothermics 37, 469–495.
IAEA. 2003. Scientific and Technical Basis for the Geological Disposal of Radioactive Wastes. https://www.iaea.org/publications/6568/scientific-and-technical-basis-for-the-geological-disposal-of-radioactive-wastes.
Itasca. 2012. FLAC3D, Fast Lagrangian Analysis of Continua in 3 Dimensions, Version 5.0. Itasca Consulting Group, Minneapolis, Minnesota.
Jaeger, J.C., Cook, N.G.W., 1979. Fundamentals of rock mechanics. Chapman and Hall, London.
Jeanne, P., Rutqvist, J., Dobson, P.F., Walters, M., Hartline, C., Garcia, J., 2014. The impacts of mechanical stress transfers caused by hydromechanical and thermal

processes on fault stability during hydraulic stimulation in a deep geothermal reservoir. Int. J. Rock Mech. Min. Sci. 72, 149–163.
Jeong, J., Kim, J.W., Cho, D.K., 2022. Optimization of spent nuclear fuels per canister to improve the disposal efficiency of a deep geological repository in Korea. Nucl. Eng. Technol. 54, 2819–2827.
Kim, I.Y., Choi, H.J., Kim, H., 2013. Evaluation on thermal performance and thermal dimensioning of direct deep geological disposal system for high burn-up spent nuclear fuel, KAERI/TR-5230/2013. Korea Atomic Energy Research Institute, Korea in Korean with English abstract.
Kim, K.I., Lee, C., Yoon, S., Cho, D., Kim, H., 2022b. Distributions of thermal performance and deposition hole spacing of high-level radioactive waste repository based on bentonite types, rock thermal properties and geothermal gradient in Korea. 3rd International Conference on Coupled Processes in Fractured Geological Media: Observation, Modeling, and Application, Berkeley, USA, November 14-16, 2022. CouFrac2022-85.
Kim, K.I., Lee, C., Kim, J.S., 2021. A numerical study of the performance assessment of coupled thermo-hydro-mechanical (THM) processes in improved Korean reference disposal system (KRS+) for high-level radioactive waste. Tunnel & Underground Space 31 (4), 221–242 in Korean with English abstract.
Kim, G.W., 1993. Revaluation of geomechanics classifications of rock masses. In: Geotechnical Engineering and Tunneling Technology, Korean Geotechnical Society Spring 93 National Conference, Seoul, Korea, pp. 33-40 (in Korean with English abstract).
F. Kober R. Schneeberger S. Vomvoris S. Finsterle B. Lanyon The HotBENT Experiment: objectives, design, emplacement and early transient evolution Geoenergy 1 1 2023 geoenergy2023-021.
Kim, K.I., Yoo, H., Park, S., Yim, J., Xie, L., Min, K.B., Rutqvist, J., 2022a. Induced and triggered seismicity by immediate stress transfer and delayed fluid migration in a fractured geothermal reservoir at Pohang, South Korea. Int. J. Rock Mech. Min. Sci. 153, 105098.
Kwon, S., Choi, J.W., 2006. Thermo-mechanical stability analysis for a multi-level radioactive waste disposal concept. Geotech. Geol. Eng. 24, 361–377.
Kwon, S., Min, K.B., 2021. Fracture transmissivity evolution around the geological repository of nuclear waste caused by the excavation damage zone, thermoshearing and glaciation. Int. J. Rock Mech. Min. Sci. 137, 104554.
Labuz, J.F., Zang, A., 2012. Mohr-Coulomb failure criterion. Rock Mech. Rock Eng. 45, 975–979.
Lee, J., Cho, D., Choi, H., Choi, J., 2007. Concept of a Korean reference disposal system for spent fuels. J. Nucl. Sci. Technol. 44 (12), 1565–1573.
Lee, J.O., Cho, W.J., 2009. Thermal-hydro-mechanical properties of reference bentonite buffer for a Korean HLW repository. KAERI/TR-3729/2009, Korea Atomic Energy Research Institute, Korea. In Korean with English Abstract.
Lee, J., Kim, I., Ju, H.J., Choi, H., Cho, D., 2020b. Proposal of an improved concept design for the deep geological disposal system of spent nuclear fuel in Korea. J. Nuclear Fuel Cycle and Waste Technology 18, 1–19.
Lee, J., Kim, K.I., Kim, I., Ju, H., Jeong, J., Lee, C., Kim, J.W., Cho, D., 2023b. High efficiency deep geological repository system for spent nuclear fuel in Korea with optimized decay heat in a disposal canister and increased thermal limit of bentonite. Nucl. Eng. Technol. 55, 1540–1554.
Lee, C., Yoon, S., Cho, W.J., Jo, Y., Lee, S., Jeon, S., Kim, G.Y., 2019. Study on thermal, hydraulic, and mechanical properties of KURT granite and Gyeongju bentonite. J. Nuclear Fuel Cycle and Waste Technology 17 (S), 65–80 in Korean with English abstract.
Lee, C., Lee, J., Park, S., Kwon, S., Cho, W.J., Kim, G.Y., 2020a. Numerical analysis of coupled thermo-hydro-mechanical behavior in single and multi-layer repository concepts for high-level radioactive waste disposal. Tunn. Undergr. Space Technol. 103 (1–17), 103452.
Lee, C., Lee, J., Lee, G.Y., 2021. Numerical analysis of coupled hydro-mechanical and thermo-hydro-mechanical behaviour in buffer materials at a geological repository for nuclear waste: Simulation of EB experiment at Mont Terri URL and FEBEX at Grimsel test site using Barcelona basic model. Int. J. Rock Mech. Min. Sci. 139, 104663.
Lee, G.J., Yoon, S., Kim, T., Chang, S., 2023a. Investigation of the various properties of several candidate additives as buffer materials. Nucl. Eng. Technol. 55, 1191–1198.
Lei, X., Ma, S., Chen, W., Pang, C., Zeng, J., Jiang, B., 2013. A detailed view of the injection-induced seismicity in a natural gas reservoir in Zigong, southwestern Sichuan Basin. China, Journal of Geophysical Research: Solid Earth 118 (8), 4296–4311.
Leupin, O.X., Smith, P., Marschall, P., Johnson, L., Savage, D., Cloet, V., Schneider, J., Senger, R., 2016. High-level waste repository-induced effects. NAGRA Technical Report 14-13. NAGRA, Switzerland.
Malmlund, H., Aikäs, K., Hagros, A., 2004. Layout adaptation examples for a KBS-3V repository at Olkiluoto. POSIVA Working Report 2003-68, POSIVA Oy, Finland.
Martin, D., 2005. Preliminary assessment of potential underground stability (wedge and spalling) at Forsmark, Simpevarp and Laxemar sites. SKB R-05-71, Swedish Nuclear Fuel and Waste Management Co., Sweden.Min, K.B., Lee, J., Stephansson, O., 2013. Implications of thermally-induced fracture slip and permeability change on the long-term performance of a deep geological repository. International Journal of Rock Mechanics & Mining Sciences 61, 275-288.
Min, K.B., Rutqvist, J., Tsang, C.F., Jing, L., 2005. Thermally induced mechanical and permeability changes around a nuclear waste repository—a far-field study based on equivalent properties determined by a discrete approach. Int. J. Rock Mech. Min. Sci. 42, 765–780.
Nagra, 2002. Demonstration of disposal feasibility for spent fuel, vitrified high-level waste and long-lived intermediate-level waste (Entsorgungsnachweis), NAGRA NTB 02–05. National Cooperative for the Disposal of Radioactive Waste, Switzerland.
Nagra, 2019. Implementation of the full-scale emplacement experiment at Mont Terri: Design, construction and preliminary results, NAGRA NTB 15–02. National Cooperative for the Disposal of Radioactive Waste, Switzerland.
K. Pruess C. Oldenburg G. Moridis TOUGH2 user's guide, Version 2.0. LBNL-43134 1999 Lawrence Berkeley National Laboratory, Berkeley, USA.
Pusch, R., Karnland, O., 1996. Physico/chemical stability of smectite clays. Eng. Geol. 41, 73–85.
Pusch, R., Bluemling, P., Johnson, L., 2003. Performance of strongly compressed MX-80 pellets under repository-like conditions. Appl. Clay Sci. 23, 239–244.
Pusch, R., Kasbohm, J., Thao, H.T.M., 2010. Chemical stability of montmorillonite buffer clay under repository-like conditions – a synthesis of relevant experimental data. Appl. Clay Sci. 47 (1–2), 113–119.
Reasenberg, A.A., Simpson, R.W., 1992. Response of regional seismicity to the static stress change produced by the Loma Prieta earthquake. Science 255, 1687–1690.
Rinaldi, A.P., Rutqvist, J., Luu, K., Blanco-Martín, L., Hu, M., Sentís, M.L., Eberle, L., Kaestli, P., 2022. TOUGH3-FLAC3D: a modeling approach for parallel computing of fluid flow and geomechanics. Comput. Geosci. 26, 1563–1580.
Rutqvist, J., 2017. An overview of TOUGH-based geomechanics models. Comput. Geosci. 108, 56–63.
Rutqvist, J., 2020. Thermal management associated with geologic disposal of large spent nuclear fuel canisters in tunnels with thermally engineered backfill. Tunn. Undergr. Space Technol. 102, 103454.
Rutqvist, J., Stephansson, O., 2003. The role of hydromechanical coupling in fractured rock engineering. Hydrgeol. J. 11, 7–40.
Rutqvist, J., Tsang, C.F., 2002. A study of caprock hydromechanical changes associated with CO_2-injection into a brine formation. Environ. Geol. 42, 296–305.
Rutqvist, J., Tsang, C.F., 2024. Modeling nuclear waste disposal in crystalline rocks at the Forsmark and Olkiluoto repository sites – Evaluation of potential thermal–mechanical damage to repository excavations. Tunn. Undergr. Space Technol. 152, 105924.
Rutqvist, J., Wu, Y.S., Tsang, C.F., Bodvarsson, G., 2002. A modeling approach for analysis of coupled multiphase fluid flow, heat transfer, and deformation in fractured porous rock. Int. J. Rock Mech. Min. Sci. 39, 429–442.
Rutqvist, J., Chijimatsu, M., Jing, L., De Jonge, J., Kohlmeier, M., Millard, A., Nguyen, T. S., Rejeb, A., Souley, M., Sugita, Y., Tsang, C.F., 2005. Numerical study of the THM effects on the near-field safety of a hypothetical nuclear waste repository – BMT1 of the DECOVALEX III project. Part 3: Effects of THM coupling in fractured rock. Int. J. Rock Mech. Min. Sci. 42, 745–755.
Rutqvist, J., Rinaldi, A.P., Cappa, F., Moridis, G.J., 2013. Modeling of fault reactivation and induced seismicity during hydraulic fracturing of shale-gas reservoirs. J. Pet. Sci. Eng. 107, 31–44.
Rutqvist, J., Zheng, L., Chen, F., Liu, H.-H., Birkholzer, J., 2014. Modeling of Coupled Thermo-Hydro-Mechanical processes with links to geochemistry associated with bentonite-backfilled repository tunnels in clay formations. Rock Mech. Rock Eng. 47, 167–186.
Seo, E., Kim, K.I., Yoo, H., Yoon, J., Min, K.B., 2024. Far-field analysis of shear slip potential and ground uplift by high-level radioactive waste repositories with single- and multi-canister and multi-layer disposal concepts. Tunelling and Underground Space Technology 145, 105611.
Skb, 2010. Choice of method – evaluation of strategies and systems for disposal of spent nuclear fuel, SKB P-10-47. Swedish Nuclear Fuel and Waste Management Co., Sweden.
Stein, R.S., 1999. The role of stress transfer in earthquake occurrence. Nature 402, 605–609.
Suzuki, K., Asano, H., Yahagi, R., Kobayashi, I., Sellin, O., Svemar, C., Holmqvist, M., 2013. Experimental investigations of piping phenomena in bentonite-based buffer materials for an HLW repository. Clay Miner. 48, 363–382.
Synn, J.H., Park, C., Lee, B.J., 2013. Regional distribution pattern and geo-historical transition of in-situ stress fields in the Korean Peninsula. Tunneling and Underground Space 23 (6), 457–469 in Korean with English abstract.
Tounsi, H., Lerche, S., Wolters, R., Hu, M., Rutqvist, J., 2023. Impact of the compaction behavior of crushed salt on the thermo-hydro-mechanical response of a generic salt repository for heat-generating nuclear waste. Eng. Geol. 323, 107217.
Trueman, R., 1988. An evaluation of strata support techniques in dual life gate roads. University of Wales, Cardiff, UK. Ph. D. Thesis,.
Villeneuve, M.C., Heap, M.J., Kushnir, A.R.L., Qin, T., Baud, P., Zhou, G., Xu, T., 2018. Estimating in situ rock mass strength and elastic modulus of granite from the Soultz-sous-Forêts geothermal reservoir (France). Geothermal Energy 6, 11.
Wersin, P., Johnson, L.H., McKinley, I.G., 2007. Performance of the bentonite barrier at temperature beyond 100 °C, A critical review. Phys. Chem. Earth 32, 780–788.
Yoon, S., Cho, W.H., Lee, C., Kim, G.Y., 2018. Thermal conductivity of Korean compacted bentonite buffer materials for a nuclear waste repository. Energies 11, 2269.
Yoon, S., Lee, G.J., Park, T.J., Lee, C., Cho, D.K., 2022. Thermal conductivity evaluation for bentonite buffer materials under elevated temperature conditions. Case Studies in Thermal Engineering 30, 101792.
K. Zhang Y.S. Wu K. Pruess User's guide for TOUGH2-MP: a massively parallel version of the TOUGH2 code 2008 Lawrence Berkeley National Laboratory Berkeley, USA Report LBNL-315E.
Zhang, X., Ma, F., Dai, Z., Wang, J., Chen, L., Ling, H., Soltanian, M.R., 2022. Radionuclide transport in multi-scale fractured rocks: a review. J. Hazard. Mater. 424, 127550.

Zhao, J., Li, H.B., Wu, M.B., Li, T.J., 1999. Dynamic uniaxial compression tests on a granite. Int. J. Rock Mech. Min. Sci. 36, 273–277.
Zheng, L., Rutqvist, J., Birkholzer, J.T., Liu, H.H., 2015. On the impact of temperatures up to 200 °C in clay repositories with bentonite engineer barrier systems: a study with coupled thermal, hydrological, chemical, and mechanical modeling. Eng. Geol. 197, 278–295.
Zheng, L., Rutqvist, J., Birkholzer, J.T., Liu, H.H., 2017. Coupled THMC models for bentonite in an argillite repository for nuclear waste: illitization and its effect on swelling stress under high temperature. Eng. Geol. 230, 118–129.